ARTICLE

Vibrational Spectra and Density Functional Theory Calculations of Metallotriphenylcorroles

Hui-ling Gao, Fang Chen, Chun-lei Wang, Guo-bing Wang, Dong-ming Chen*

Department of Chemical Physics, University of Science and Technology of China, Hefei 230026, China

(Dated: Received on April 27, 2013; Accepted on May 14, 2013)

The infrared absorption and Raman scattering spectra were measured for the metallotriphenylcorroles (MTPCs, M=Cu, Co, Ni, Mn). The ground-state structures and vibrational spectra of MTPCs have been calculated with the density functional theory. The observed Raman and IR bands have been assigned based on the calculation results. Due to the symmetry lowering, the vibrational spectra of MTPCs are much more complex than metalloporphyrins, and several skeletal modes are found strongly coupled to the phenyl vibrations. The relationship between the Raman/IR frequencies and the structures of TPC ring is investigated. It is found that the vibrations involving the $C_\alpha^I C_\alpha^I$ stretch and $C_\alpha C_m$ stretch are sensitive to the size of corrole core. In particular, the frequency of ν_5, which is assigned to $C_\alpha^I C_\alpha^I$ stretch in coupling with the $C_\alpha C_m$ symmetric stretch, increases linearly with the decrease of the corrole core-sizes and may be used as a mark band to evaluate the structural change of the metallocorroles.

Key words: Metallocorroles, Raman spectrum, Molecular vibration, Density functional theory

I. INTRODUCTION

The corroles as a member of the porphyrinoid family are very important multifunctional compounds. Owing to their unique properties in chemistry and photochemistry, the corroles have great application prospects in a wide range of areas from catalyst, electrochemistry, bio-sensors, nonlinear optics, to photodynamic therapy of tumor [1−3]. They are also used as the structural model of corrin, the core component of vitamin B12. In comparison with normal porphyrins and other related macrocyclces, an important feature of the corrole ligands is their capability of stabilizing high oxidation states for coordinated metal ions, due to bearing three ammoniac nitrogen atoms [4−7]. As a result of their unique coordination chemistry, the metallocorroles show distinct catalytic properties for the oxidation or hydroxylation of hydrocarbons [8−11]. For these reasons, the studies of corroles have now become one of the most active branches of porphyrin chemistry. Numerous transition-metal and main-group metal complexes of the corroles have been synthesized and spectroscopically characterized [4−18]. It has been found that the periphery substituents have a significant influence on the electrochemical properties and the electronic absorption spectra of metallocorroles (MCors) [14−16]. For instance, the Soret bands of copper corroles with different triaryl substituents have been found shift as large as 100 nm [16]. It is clear that periphery modification of the metallocorroles can be an effective route to manipulate their electronic and optical properties.

Raman and IR spectra play an important role in the structural and dynamic studies of porphyrin-related compounds. Theoretically, the density functional theory (DFT) calculations have been widely used to study the vibrational spectra of porphyrin-related compounds in recent years, proven useful in revealing information about the structures and vibrational states of these compounds [19−25]. Although vibrational spectra [17, 18] and DFT calculations [26−30] of several metallocorroles have been reported, descriptions of vibrational modes of metallocorroles, especially the meso-substitued metallocorroles, are still not fully understood.

In this work, we report IR and Raman spectroscopic properties of series metal complexes of meso-triphenylcorrole (MTPC, M=Cu, Ni, Co, and Mn) together with DFT calculations to obtain more detailed knowledge about the vibrational states of these complexes.

II. EXPERIMENTAL AND COMPUTATIONAL METHODS

The synthesis of free-base meso-triphenylcorrole (H_3TPC) was adapted from the method by Koszarna and Gryko [31]. 200 mL distilled water and 20 mL methanol was mixed in a flask, then 10 mmol freshly

*Author to whom correspondence should be addressed. E-mail: dmchen@ustc.edu.cn, Tel.: +86-551-63606145

distill pyrrole and 5 mmol benzoic aldehyde and 4.25 mL hydrochloric acid (36%) were added into the solvent. After stirring for 3 h at room temperature, the reactant was extracted with chloroform. The organic layer was washed twice with distilled water, dried with anhydrous Na_2SO_4, and then filtrated with diatomite. The obtained solution was diluted to 300 mL with chloroform in a flask to react with 1.23 g (5 mmol) chloranil for 1 h at room temperature. The resultant was chromatographic separated on a silica gel colume washed with dichloromethane first and then with 1:1 mixed dichloromethane/*n*-hexane flow phase. The green component was collected. After evaporation of the solvent, the black-green target product was obtained.

The metal complexes, MTPC (M=Cu, Ni, Co, Mn), were synthesized according to the method in Ref.[32], *i.e.*, by treating the metal-acetates and free base H_3TPC in hot chloroform/methanol mixture (7:3 in volume). Taking nickel complex (NiTPC) as an instance, the synthesis details are as follows. Reagent-grade chloroform/methanol mixture (10 mL) was brought gently to a reflux on a hot plate and magnetically stirred to 60 °C. The solid H_3TPC (10 mg) was added into the solvent and allowed to dissolve completely for a few minutes. Then excess nickel acetate ($Ni(CH_3COO)_2{\cdot}4H_2O$) was added into the solution. Reaction proceeded for about 1 h to allow complete conversion from the free base to the nickel complex. After the reaction mixture cooled, equal volume of distilled water was added into the reaction mixture to precipitate the NiTPC species. The product was separated with a centrifuge and washed with water to remove unreacted nickel acetate. The centrifuging and washing procedures repeated several times until the up-layer solution is clear. The obtained solid NiTPC sample was then silica-gel dried in a desiccator. Similar procedures were carried out to prepare the copper, cobalt, and manganese complexes.

IR spectra of MTPC were measured on a Nicolet MAGNA-IR750 infrared spectrometer as KBr pellets. Raman spectra of MTPC solid powders were measured on a Labram-010 micro-Raman spectrometer. The 488.0 nm line of an Ar^+ laser (Spectra-Physics 163-C12) was used as the excitation source with the power of 7 mW on samples. The time constant of the air-cooled CCD detector was 15 s, and 4 scans were accumulated for each Raman spectrum.

DFT calculations for the structural optimizations of MTPC were carried out by using the Becke's three-parameter hybrid functional (referred as B3LYP) [33]. Standard 6-31G(d) basis sets were used for C, N, and H, while Ahlrichs' TZVP basis sets for Cu, Ni, Co, and Mn [34]. Frequency calculations at the optimized geometries were conducted to confirme the structure as an energy minimum (with all the frequencies to be positive values) as well as to obtain the theoretical IR and Raman spectra. Assignment of individual vibrational frequency has been carried out by inspecting the calculated Cartesian displacements of the corresponding normal mode. As DFT-calculations are known to systematically overestimate harmonic frequencies, the resultant theoretical frequencies are scaled with a single factor of 0.97. The same factor has been used in the DFT calculations of metalloporphyins and other tetrapyrrole compounds [22−25]. All calculations were performed with the Gaussion 09 [35] program suite on the Lenova 1800 supercomputer of USTC supercomputation center.

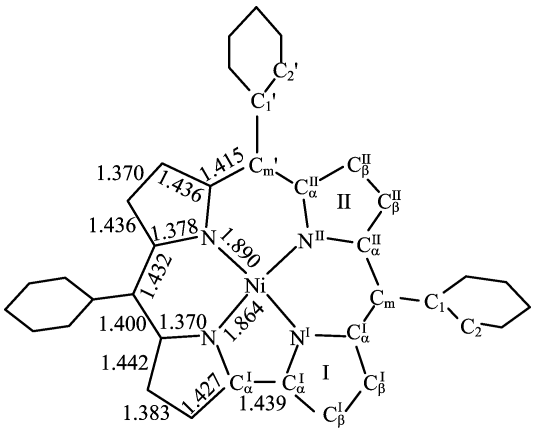

FIG. 1 Structural sketch of NiTPC with atomic labels. The four pyrrole rings are divided into two types (I and II).

III. RESULTS AND DISCUSSION

A. Geometries and general consideration of the molecular vibrations of MTPCs

Geometry optimizations have been carried out for MTPCs (M=Cu, Ni, Co, and Mn) with various spin-multiplicities. Computational results indicate that the ground state spin-multiplicity is doublet for NiTPC, triplet for CuTPC and CoTPC, and quintet for MnTPC. The ground state structures of all the four complexes are C_2 symmetry with the corrole skeleton to be nearly planar. The maximum derivation of the skeletal atoms from the corrole mean-plane is 0.064 Å for CuTPC, 0.037 Å for NiTPC, 0.032 Å for CoTPC, and 0.043 Å for MnTPC. The M−N bond lengths, which measure the size of the coordination core, are 1.925/1.928 Å for CuTPC, 1.864/1.890 Å for NiTPC, 1.853/1.877 Å for CoTPC, 1.905/1.913 Å for MnTPC.

Figure 1 displays the structure sketch and the atomic labels of NiTPC with some key structural parameters, in which the four pyrrole rings are divided into two sets, denoted as Pyr-I and Pyr-II respectively, with taking the C_2 symmetry into account. The atoms of corrole skeleton are thereby denoted as C^{I}_{α}, C^{I}_{β}, C^{II}_{α}, C^{II}_{β}, N^{I}, N^{II}, C_m (at the two symmetric methines), and C'_m (at the isolated methine). The phenyl groups of MTPCs are inclined with respect of the corrole mean-plane. For NiTPC, the dihedral angles between the

DOI:10.1063/1674-0068/26/04/398-408

mean planes of phenyl groups and the corrole skeleton are 49.6° (for C_m-phenyl groups) and 64.5° (for C'_m-phenyl). Since the calculated ground state structures and the IR and Raman spectra of the four complexes show similar trends, our discussions in the following sections will be concentrated on NiTPC.

Customarily, a simplified planar molecular model, in which all peripheral substituents are represented by point masses, is often used in the vibrational analyses of the porphyrins and other tetrapyrrole macrocycles for convenience [19−25, 36, 37]. The molecular vibrations of a tetrapyrrole compound can thus be divided into the macrocyclic skeletal modes and the substituent internal modes despite the fact that the motions of the skeletal atoms and the substituent atoms may correlate with each other. The vibrations of macrocyclic skeleton can be further divided into the in-plane (ip) and the out-of-plane (oop) types. With this strategy, the skeleton of a metallocorrole (MCor) can be assumed having a planar C_{2v} structure and its skeletal modes can be classified as:

$\Gamma_{\text{MCor-ip}}=34A_1+33B_2$

$\Gamma_{\text{MCor-oop}}=15A_2+17B_1$

For MTPC which has a reduced C_2 symmetry, the skeletal modes should be classified according to the irreducible representations of the C_2 point group:

$\Gamma_{\text{MTPC-ip}}=34A+33B$

$\Gamma_{\text{MTPC-oop}}=15A+17B$

The phenyl internal modes, according to the atomic motions in or out of the phenyl planes, can be classified as:

$\Gamma_{\text{Ph-ip}}=30A+30B$

$\Gamma_{\text{Ph-oop}}=14A+16B$

In the following senctions, the IR/Raman bands of MTPC will be assigned to local coordinates in which the phasing of adjacent bond stretches within the pyrrole rings and at the meso-carbon bridges are taken into account [21, 25, 36, 37]. The local coordinates of MTPC in this work follow those used in metalloporphyrins as defined by Li *et al.* [36, 37]. For in-plane vibrations, the stretches of $C_mC_1/C'_mC'_1$, $C^I_\beta H/C^{II}_\beta H$, and $C^I_\beta C^I_\beta/C^{II}_\beta C^{II}_\beta$ bonds and the in-plane bending of $C^I_\beta H/C^{II}_\beta H$ are defined as isolated local coordinates. The stretch of $C^I_\alpha C^I_\alpha$ bond that connects the adjacent Pyr-I rings is also defined as an isolated local coordinate. The stretches of adjacent $C_\alpha C_m$ bonds are defined as symmetric and asymmetric, respectively, depending on in-phase or out-of-phase. As the stretches of $C^I_\alpha C^I_\beta/C^{II}_\alpha C^{II}_\beta$ and $C^I_\alpha N^I/C^{II}_\alpha N^{II}$ bonds in the same pyrrole ring are heavily coupled with each other, the corresponding vibrations are defined as pyrrole quarter-ring, symmetric half-ring, asymmetric half-ring, and pyrrole breathing coordinates. The vibrations involving mainly the bending of the pyrrole bond-angles are defined as pyrrole symmetric and asymmetric deformations. For the out-of-plane vibrations, local coordinates are defined as pyrrole symmetric or asymmetric folding, pyrrole swivel, pyrrole tilting *etc.* The atomic motions for these local coordinates can be found in Ref.[36, 37]. The vibrations of phenyl groups can be classified into two types, in-plane and out-of-plane modes, respectively, each of which is further divided into symmetric or asymmetric with respect to the reflection of the plane that is perpendicular to the phenyl plane and passes the $C_mC_1/C'_mC'_1$ bond. The phenyl modes are thereby denoted as φ(in-plane symmetric), ψ(in-plane asymmetric), π(out-of-plane symmetric), and σ(out-of-plane asymmetric).

The calculated vibrational frequencies of NiTPC and their local coordinate descriptions are listed in the Tables I−IV. Our calculations indicate that the molecular vibrations of NiTPC show some similarity to nickel meso-tetraphenylporphyrin (NiTPP), the porphyrin counterpart of NiTPC. The frequencies in the 1440−1600 cm^{-1} region involve mainly the stretches of $C_\beta C_\beta$, $C_\alpha C_m$ bonds of corrole ring and CC bonds of phenyl groups. The $C_\beta H$ in-plane bending and several pyrrole $C_\alpha C_\beta/C_\alpha N$ stretches are located in the 1040−1280 cm^{-1} region. The frequencies lower than 970 cm^{-1} are mainly due to the out-of-plane vibrations of corrole skeleton and phenyl groups. On the other hand, IR and Raman spectra of NiTPC are more complex compared with NiTPP. This is expectable since the symmetry breaking of NiTPC causes splitting of the degenerated vibrational states and relaxation of IR and Raman selection rules. In addition, the vibrational coupling between the phenyl groups and the macrocycle is stronger in NiTPC than that in NiTPP, which results from the quite sharp dihedral angles between the C_m-phenyl groups and the corrole macrocycle (49.6°). In the following sections, assignments of the observed IR/Raman bands of NiTPC to local coordinates are discussed.

B. Vibrational spectra of NiTPC

Figure 2 shows the experimental IR spectra of NiTPC in KBr pellets, in which the theoretical IR spectrum by B3LYP calculations is also provided (harmonic frequencies scaled with 0.97). It can be seen from Fig.2 that the experimental and the theoretical spectra are coincident with each other in general. By comparing with the DFT-calculated band positions and intensities, the observed IR bands of NiTPC and other three complexes are assigned as listed in Table V. While both A and B modes are IR active, most of the strong IR absorptions of NiTPC in the high frequency region (900−1600 cm^{-1}) belong to the A symmetry. Most of the IR bands with frequencies larger than 900 cm^{-1} come from the in-plane corrole skeletal vibrations while the out-of-plane skeletal vibrations and phenyl modes dominate the region of 400−900 cm^{-1}. In 1400−1650 cm^{-1}, IR bands were measured at 1578, 1530, 1516, 1497, 1464, and 1440 cm^{-1}. Theoretically, IR bands were predicted at 1608, 1582, 1523, 1496, 1465, and 1435 cm^{-1}. The 1578 cm^{-1} band can be as-

DOI:10.1063/1674-0068/26/04/398-408

TABLE I Calculated in-plane skeletal modes (frequencies in cm^{-1}) of NiTPC[a].

A symmetry			B symmetry		
No.	Frequency	Mode description[b]	No.	Frequency	Mode description[b]
ν_1	3191	$\nu(C_\beta^{II}H)_s$	ν_{35}	3191	$\nu(C_\beta^{II}H)_s$
ν_2	3180	$\nu(C_\beta^{I}H)_s$	ν_{36}	3180	$\nu(C_\beta^{I}H)_s$
ν_3	3175	$\nu(C_\beta^{II}H)_{as}$	ν_{37}	3175	$\nu(C_\beta^{II}H)_{as}$
ν_4	3160	$\nu(C_\beta^{I}H)_{as}$	ν_{38}	3159	$\nu(C_\beta^{I}H)_{as}$
ν_5	1532	$\nu(C_\alpha^{I}C_\alpha^{I})+\nu(C_\alpha{}^{I,II}C_m)_s$	ν_{39}	1518	$\nu(C_\alpha^{I,II}C_m)_{as}$
ν_6	1523	$\nu(C_\alpha^{I,II}C_m)_{as}+\nu$(Pyr-I/2)$_{as}$	ν_{40}	1482	$\nu(C_\beta^{I}C_\beta^{I})+\nu(C_\beta^{II}C_\beta^{II})$
ν_7	1499	$\nu(C_\alpha^{II}C'_m)_s$	ν_{41}	1465	$\nu(C_\beta{}^{II}C_\beta^{II})+\nu(C_\beta^{I}C_\beta^{I})$
ν_8	1459	$\nu(C_\beta^{I}C_\beta^{I})$	ν_{42}	1459	$\nu(C_\alpha^{II}C'_m)_{as}$
ν_9	1435	$\nu(C_\beta^{II}C_\beta^{II})$	ν_{43}	1428	$\nu(C_\alpha^{I,II}C_m)_s$
ν_{10}	1416	$\nu(C_\alpha^{I,II}C_m)_s$	ν_{44}	1371	ν(Pyr-I/4)
ν_{11}	1374	ν(Pyr-II/2)$_s+\nu$(Pyr-I/2)$_s$	ν_{45}	1337	ν(Pyr-I/2)$_s+\nu$(Pyr-II/4)
ν_{12}	1345	ν(Pyr-I/4)	ν_{46}	1320	ν(Pyr-I/4)$+\nu$(Pyr-II/2)$_{as}$
ν_{13}	1333	ν(Pyr-I/2)$_s$	ν_{47}	1316	ν(Pyr-II/2)$_s$
ν_{14}	1297	ν(Pyr-II/4)	ν_{48}	1262	$\nu(C_mC_1)+\nu$(Pyr-II/4)
ν_{15}	1276	$\delta(C_\beta^{I}H)_{as}$	ν_{49}	1221	$\delta(C_\beta^{I}H)_{as}$
ν_{16}	1258	$\nu(C_mC_1)+\nu$(Pyr-II/4)	ν_{50}	1154	ν(Pyr-I/2)$_{as}$
ν_{17}	1224	$\nu(C'_mC'_1)$	ν_{51}	1132	$\delta(C_\beta^{I}H)_{as}$
ν_{18}	1189	$\delta(C_\beta^{II}H)_{as}$	ν_{52}	1072	$\delta(C_\beta^{II}H)_s$
ν_{19}	1082	$\delta(C_\beta^{II}H)_s$	ν_{53}	1049	$\delta(C_\beta^{II}H)_s$
ν_{20}	1059	$\delta(C_\beta^{I}H)_s$	ν_{54}	1025	ν(Pyr-II br.)
ν_{21}	1028	ν(Pyr-I/2)$_{as}$	ν_{55}	1013	ν(Pyr-II/2)$_{as}$
ν_{22}	1017	ν(Pyr-II br.)	ν_{56}	983	ν(Pyr-I br.)
ν_{23}	1017	ν(Pyr-II/2)$_{as}$	ν_{57}	889	δ(Pyr-I def.)$_s$
ν_{24}	984	ν(Pyr-I br.)	ν_{58}	863	δ(Pyr-I def.)$_{as}+\delta$(Pyr-II def.)$_s$
ν_{25}	878	ν(Pyr-II def.)$_s+\nu$(Pyr-I def.)$_{as}$	ν_{59}	835	δ(Pyr-I def.)$_s+\delta$(Pyr-II def.)$_{as}$
ν_{26}	870	ν(Pyr-II def.)$_{as}$	ν_{60}	806	(Pyr-I def.)$_{as}+\delta$(Pyr-II def.)$_{as}$
ν_{27}	835	ν(Pyr-I def.)$_{as}+\nu$(Pyr-II def.)$_{as}$	ν_{61}	553	δ(Pyr-I rot.)
ν_{28}	525	δ(Pyr-I transl)$+\delta$(Pyr-II transl)	ν_{62}	471	δ(Pyr-II rot.)
ν_{29}	476	ν(NiN)	ν_{63}	431	δ(Pyr-I transl.)$+\delta$(Pyr-II transl.)
ν_{30}	421	δ(Pyr-I rot.)$+\delta$(Pyr-II rot.)	ν_{64}	332	δ(Pyr-II transl.)$+\delta$(Pyr-I transl.)
ν_{31}	408	δ(Pyr-II transl.)$+\delta$(Pyr-I transl.)	ν_{65}	288	ν(NiN)
ν_{32}	385	ν(NiN)	ν_{66}	270	$\delta(C_m$-Ph)
ν_{33}	313	δ(Pyr-I rot.)$+\delta$(Pyr-II rot.)	ν_{67}	244	$\delta(C_m$-Ph)
ν_{34}	239	$\delta(C_m$-Ph)			

[a] Calculated with B3LYP, basis sets: 6-31G* for C, N, and H, TZVP for Ni. Frequency scaling factor is 0.97.
[b] For more than one local coordinates listed, the first one is dominate. "I" and "II" represent pyrrole ring I and II, respectively. "s"-symmetric, "as"-asymmetric, the description of local coordinates is according to Refs.[36, 37].

signed to the asymmetric CC stretching mode of phenyl substituents (ψ'_3), which is calculated at 1582 cm^{-1}. Another phenyl mode calculated at 1608 cm^{-1} (φ_4) is not observed in the experimental spectrum.

The stretching vibrations of $C_\beta C_\beta$, $C_\alpha C_m$, and $C_\alpha^I C_\alpha^I$ bonds are expected to appear in the 1440−1650 cm^{-1} region due to their relatively large force constants. The 1497 cm^{-1} band in the experimental spectrum is thought to correspond to the 1496 cm^{-1} band in the theoretic spectrum and is assigned to φ_5, the CC stretch and CH bending of the phenyl groups. The absorption band observed at 1464 cm^{-1} is considered to correspond to the calculated band at 1465 cm^{-1}, which according to the DFT calculation is a corrole skeletal mode (ν_{41}) involving the stretches of $C_\beta^I C_\beta^I$ and $C_\beta^{II} C_\beta^{II}$ bonds, and weakly, the $C_\alpha^{I,II} C_m$ asymmetric stretch. The IR band observed at 1440 cm^{-1} is thought to correspond to the calculated band at 1435 cm^{-1} (ν_9). Calculations reveal that this band is due to the $C_\beta^{II} C_\beta^{II}$ stretch that is

DOI:10.1063/1674-0068/26/04/398-408

TABLE II Calculated out-of-plane skeletal modes (frequencies in cm^{-1}) for NiTPC[a].

A symmetry			B symmetry		
No.	Frequency	Mode description[b]	No.	Frequency	Mode description[b]
γ_1	881	$\gamma(C_\beta^{II}H)_{as}$	γ_{16}	881	$\gamma(C_\beta^{II}H)_{as}$
γ_2	854	$\gamma(C_\beta^{I}H)_{as}$	γ_{17}	854	$\gamma(C_\beta^{I}H)_{as}$
γ_3	773	γ(Pyr-II fold)$_s$	γ_{18}	777	γ(Pyr-II fold)
γ_4	762	γ(Pyr-I fold)$_s$	γ_{19}	755	γ(Pyr-I fold)$_s$
γ_5	706	$\gamma(C_\beta^{II}H)_s$	γ_{20}	708	$\gamma(C_\beta^{II}H)_s$
γ_6	700	$\gamma(C_\beta^{I}H)_s$	γ_{21}	706	$\gamma(C_\beta^{I}H)_s$
γ_7	656	γ(Pyr-II fold)$_{as}$+γ(Pyr-I fold)$_{as}$	γ_{22}	648	γ(Pyr-II fold)$_{as}$+γ(Pyr-I fold)$_{as}$
γ_8	647	γ(Pyr-I fold)$_{as}$+γ(Pyr-II fold)$_{as}$	γ_{23}	626	γ(Pyr-I fold)$_{as}$+γ(Pyr-II fold)$_{as}$
γ_9	562	$\gamma(C_\alpha^{I,II}C_m)$+$\gamma(C_\alpha^{II}C'_m)$	γ_{24}	569	$\gamma(C\alpha^{I,II}C_m)$+$\gamma(C\alpha^{II}C'_m)$
γ_{10}	365	γ(Pyr-I swivel)	γ_{25}	564	$\gamma(C_\alpha^{II}C'_m)$
γ_{11}	300	γ(Pyr-II swivel)	γ_{26}	317	γ(Pyr-II swivel)
γ_{12}	250	γ(Pyr tilt)	γ_{27}	297	γ(Ni-N)
γ_{13}	154	γ(Pyr tilt)	γ_{28}	258	γ(Pyr-I swivel)
γ_{14}	150	$\gamma(C_m$-Ph)	γ_{29}	203	γ(Pyr tilt)
γ_{15}	89	γ(Pyr transl.)	γ_{30}	156	γ(Pyr tilt)
			γ_{31}	113	$\gamma(C_m$-Ph)
			γ_{32}	92	$\gamma(C_m$-Ph)

[a] Calculated with B3LYP, basis sets: 6-31G* for C, N, and H, TZVP for Ni. Frequency scaling factor is 0.97.
[b] For more than one local coordinates listed, the first one is dominate. "I" and "II" represent pyrrole ring I and II, respectively. "s"-symmetric, "as"-asymmetric, Refs.[36, 37] for the description of local coordinates.

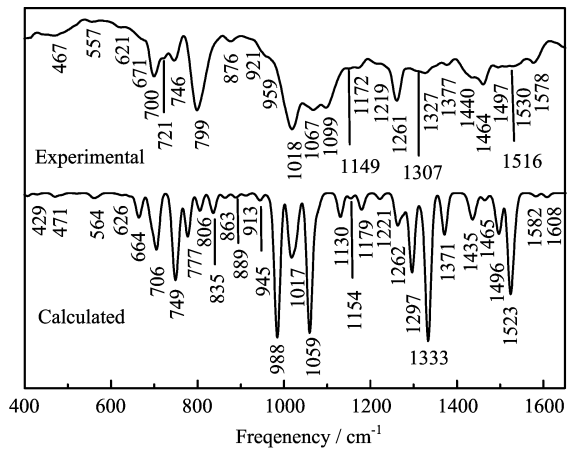

FIG. 2 Experimental (KBr disc) and calculated (frequency scaling factor is 0.97) IR absorption spectra of NiTPC.

strongly coupled to the $C_\beta^I C_\beta^I$ stretch and symmetric $C_\alpha^{II}C'_m$ stretch. Two weak bands were observed at 1530 and 1516 cm^{-1} respectively. Theoretical calculation reveals a strong band at 1523 cm^{-1} (ν_6). The ν_6 mode can be assigned to the asymmetric $C_\alpha^{I,II}C_m$ stretch (A symmetry). The DFT calculation also manifests that this mode is strongly mixed with the half-ring asymmetric stretch of Pyr-I.

In the region of 900−1440 cm^{-1}, the strongest absorption was observed at 1018 cm^{-1} in the IR spectrum of NiTPC. However, DFT calculation predicts two strong IR bands at 1017 and 988 cm^{-1}, respectively. The broad 1017 cm^{-1} band contains IR absorptions of four skeletal vibrations, *i.e.*, ν_{21}, ν_{22}, ν_{23}, and ν_{55}, with ν_{22} dominating IR intensity. The calculated 988 cm^{-1} can be assigned to φ_8, the breathing vibration of the C_m-phenyl groups. We find that in this mode the vibrational coupling between the C_m-phenyl groups and the corrole skeleton is very severe. Since several strong IR absorptions are predicted in nearby positions, it is difficult to give a definite assignment of the observed 1018 cm^{-1} band. We tend to attributing it to either ν_{22} or φ_8.

Other strong absorption bands were observed at 1261, 1099, and 1067 cm^{-1}. The 1262 cm^{-1} band is thought to correspond to the calculated band at 1262 cm^{-1} (ν_{48}), which is assigned to C_m-C_1 stretch that is weakly coupled quarter-ring stretch of Pyr-II. The 1099 cm^{-1} band is assigned to phenyl in-plane CH bending ψ_8 that is calculated at 1080 cm^{-1} as a shoulder band. The 1067 cm^{-1} band in the experimental spectrum is thought due to ν_{20} (symmetric bending of $C_\beta^I H$ bond) which is calculated at 1059 cm^{-1} with a large IR intensity. Additional weak absorption bands were observed at 1377, 1327, 1307, 1219, 1172, 1149, 959, and 921 cm^{-1}. The calculated frequencies for these bands are at 1371 (ν_{44}), 1333 (ν_{13}), 1297 (ν_{14}), 1221 (ν_{49}),

DOI:10.1063/1674-0068/26/04/398-408

TABLE III Calculated in-plane phenyl modes for NiTPC[a].

A symmetry			B symmetry		
No.	f[b]	Md[c]	No.	f[b]	Md[c]
φ_1	3121	ν(CH)	φ'_1	3121	ν(CH)
φ''_1	3120	ν(CH)	ψ_1	3116	ν(CH)
ψ'_1	3116	ν(CH)	ψ''_1	3115	ν(CH)
φ_2	3109	ν(CH)	φ'_2	3109	ν(CH)
φ''_2	3108	ν(CH)	ψ'_2	3098	ν(CH)
ψ_2	3098	ν(CH)	ψ''_2	3098	ν(CH)
φ_3	3090	ν(CH)	φ'_3	3090	ν(CH)
φ''_3	3090	ν(CH)	φ''_4	1607	ν(CC)
φ_4	1608	ν(CC)	ψ_3	1583	ν(CC)
φ'_4	1607	ν(CC)	ψ''_3	1582	ν(CC)
ψ'_3	1582	ν(CC)	φ_5	1496	ν(CC)+δ(CH)
φ'_5	1495	ν(CC)+δ(CH)	ψ_4	1443	ν(CC)+δ(CH)
φ''_5	1492	ν(CC)+δ(CH)	ψ''_4	1440	ν(CC)+δ(CH)
ψ'_4	1440	ν(CC)+δ(CH)	ψ_5	1325	δ(CH)
ψ''_5	1325	δ(CH)	ψ'_5	1325	δ(CH)
ψ_6	1293	δ(CH)	ψ'_6	1292	δ(CH)
φ_6	1179	δ(CH)	ψ''_6	1287	δ(CH)
φ''_6	1178	δ(CH)	φ'_6	1179	δ(CH)
ψ'_7	1158	δ(CH)	ψ_7	1158	δ(CH)
ψ'_8	1079	δ(CH)	ψ''_7	1157	δ(CH)
φ_7	1047	δ(CH)	ψ_8	1080	δ(CH)
φ'_7	1038	δ(CH)	ψ''_8	1078	δ(CH)
φ'_8	986	Ph. br.	φ''_7	1030	δ(CH)
φ''_8	986	Ph. br.	φ_8	988	Ph. br.
φ_9	670	δ(CCC)	φ'_9	664	δ(CCC)
φ''_9	643	δ(CCC)	ψ_9	616	δ(CCC)
ψ'_9	615	δ(CCC)	ψ''_9	615	δ(CCC)
φ_{10}	206	δ(CCC)	φ'_{10}	223	δ(CCC)
φ''_{10}	201	δ(CCC)	ψ'_{10}	32	Ph. rock.
ψ_{10}	51	Ph. rock.	ψ''_{10}	19	Ph. rock.

[a] Calculated with B3LYP, basis sets: 6-31G* for C, N, and H, TZVP for Ni. Frequency scaling factor is 0.97.
[b] f denotes frequencies in cm^{-1}.
[c] Md denotes mode description.

TABLE IV Calculated out-of-plane phenyl modes for NiTPC[a].

A symmetry			B symmetry		
No.	f[b]	Md[c]	No.	f[b]	Md[c]
π_1	968	γ(CH)	π'_1	968	γ(CH)
σ_1	945	γ(CH)	π''_1	967	γ(CH)
σ''_1	943	γ(CH)	σ'_1	945	γ(CH)
π'_2	913	γ(CH)	π_2	913	γ(CH)
σ_2	839	γ(CH)	π''_2	911	γ(CH)
σ''_2	837	γ(CH)	σ'_2	839	γ(CH)
π_3	749	γ(CH)	π'_3	747	γ(CH)
π'_4	694	γ(CCC)	π''_3	743	γ(CH)
π''_5	470	γ(CCC)	π_4	693	γ(CCC)
σ'_3	406	γ(CCC)	π''_4	692	γ(CCC)
σ''_3	404	γ(CCC)	π_5	517	γ(CCC)
σ'_4	56	Ph. spin.	π'_5	482	γ(CCC)
π'_6	54	Ph. rock.	σ_3	407	γ(CCC)
σ''_4	37	Ph. spin.	π_6	81	Ph. rock.
			σ_4	62	Ph. spin.
			π''_6	50	Ph. rock.

[a] Calculated with B3LYP, basis sets: 6-31G* for C, N, and H, TZVP for Ni. Frequency scaling factor is 0.97.
[b] f denotes frequencies in cm^{-1}.
[c] Md denotes mode description.

1179 (φ'_6), 1154 (ν_{50}), 945 (σ'_1), and 913 cm^{-1} (π_2). According to DFT calculated atomic Cartesian displacements, ν_{44}, ν_{13}, ν_{14}, ν_{49}, and ν_{50} are the corrole skeletal modes, corresponding to the quarter-ring stretch of Pyr-I, symmetric half-ring stretch of Pyr-I, quarter-ring stretch of Pyr-II, asymmetric $C^{I}_{\beta}H$ in-plane bending, and asymmetric half-ring stretch of Pyr-I, respectively. The φ'_6, σ'_1, and π_2 are the phenyl modes which involve mainly the in-plane CH bending (φ'_6) and out-of-plane CH wag (σ'_1 and π_2) of the phenyl groups.

In the low frequency region (<900 cm^{-1}), strong IR bands were measured at 799, 746, 721, and 700 cm^{-1} while strong or middle strong absorptions were calculated at 835 (ν_{59}), 806 (ν_{60}), 777 (γ_{18}), 749 (π_3), and 706 cm^{-1}. We tentatively assign the 799 cm^{-1} band to ν_{60}, the asymmetric deformation of Pyr-I which couples with asymmetric deformation of Pyr-II. It seems that γ_{18} may also contribute to the 799 cm^{-1} band as it is a rather broad absorption. The π_3 mode is due to the CH out-of-plane wag of the phenyl groups and is believed corresponding to the observed 746 cm^{-1} band. The calculated strong absorption at 706 cm^{-1} comes from the overlap of several normal modes, *i.e.*, γ_5, γ_6, γ_{20}, and γ_{21}, which belong to the out-of-plane wag of $C^{I}_{\beta}H$ and $C^{II}_{\beta}H$ bonds and are calculated at 708, 706, 706, and 700 cm^{-1} respectively. The observed IR band at 700 cm^{-1} is assigned to γ_{21} since this mode was predicted by calculations to have strongest intensity among the four modes. The observed shoulder at 721 cm^{-1} is assigned to γ_{20} that is of a higher frequency than γ_{21}.

Weak IR bands were observed at 876, 671, 621, 557, and 467 cm^{-1}, respectively. They are assigned to ν_{58} (the deformation of pyrrole rings), φ'_9, φ''_9 (in plane deformation of phenyl groups), γ_{25} (out-of-plane wag of the C'_m atom), and ν_{62} (the in-plane rotation of Pyr-II rings), respectively. These modes were calculated at 863, 664, 643, 564, and 471 cm^{-1}, respectively.

Figure 3 compares the 488.0 nm excited Raman spectrum of NiTPC (solid powder) with the DFT calculated Raman spectrum. Observed Raman frequencies of NiTPC and other three complexes are listed in Table VI together with their assignments. It can be seen from it that most of the strong Raman bands belong to

DOI:10.1063/1674-0068/26/04/398-408

TABLE V Observed IR frequencies (in cm^{-1}) of MTPCs and their assignments. IR spectra were obtained with KBr discs.

	NiTPC	CuTPC	CoTPC	MnTPC		NiTPC	CuTPC	CoTPC	MnTPC
φ_4'		1593		1591	ν_{22}/φ_8	1018	1017	1015	1022
ψ_3'	1578	1553	1578	1571	ν_{24}		979	991	982
ν_{39}	1530	1525	1541	1542	σ_1'	959		951	
ν_6	1516	1515		1513	π_2	921	929	921	928
φ_5	1497	1490	1491	1490	ν_{57}		890	889	
ν_{41}	1464	1464	1464	1459	ν_{58}	876	873	880	876
ν_9	1440	1443	1444	1436	γ_2		842		841
ν_{43}		1420	1418	1420	ν_{59}		823	824	814
ν_{44}	1377	1361	1371	1358	ν_{60}	799	789	793	792
ν_{13}	1327	1336	1350	1336	π_3	746	752	748	752
ν_{14}	1307	1306	1312	1301	γ_{20}	721	714	718	717
ν_{48}	1261	1267	1263	1282	γ_{21}	700	703	696	698
ν_{16}		1239	1239	1260	φ_9'	671	672		668
ν_{49}	1219		1214	1215	γ_{22}		654		650
φ_6'	1172	1174	1175	1177	φ_9''	621	617	619	623
ν_{50}	1149	1155	1158	1152	γ_{25}	557	577	563	573
ν_{51}		1120	1128		ν_{28}		518	515	523
ψ_8	1099	1097	1099	1107	ν_{62}	467	476	469	482
ν_{20}	1067	1057	1059	1053	ν_{63}		453		458

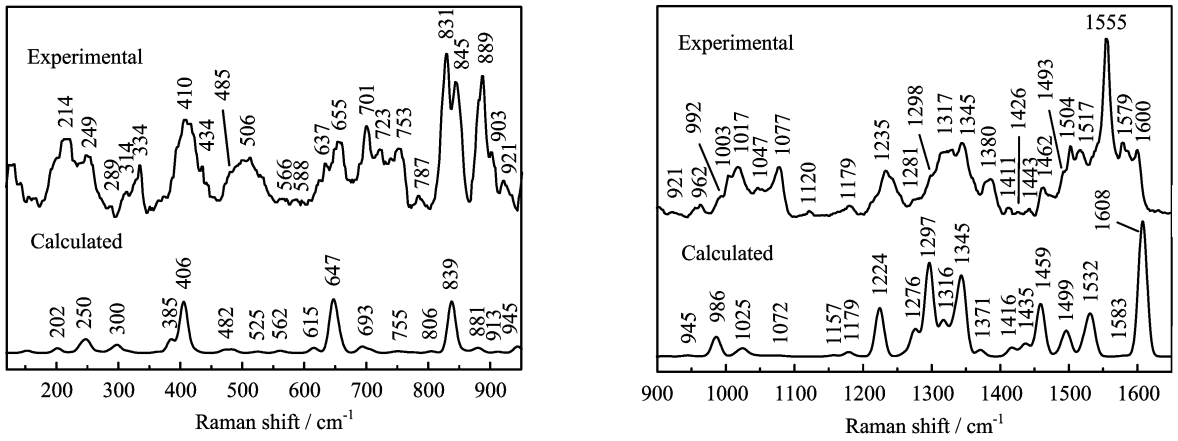

FIG. 3 Experimetal (solid powder with 488 nm excitation) and calculated (frequency scaling factor is 0.97) Raman spectra of NiTPC.

A symmetry, although both A and B modes are Raman active.

As shown in Fig.3, the 488.0 nm excited spectrum of NiTPC gives rise to eight bands in 1440−1650 cm^{-1} region, at 1600, 1579, 1555, 1517, 1504, 1493, 1462, and 1443 cm^{-1}, respectively. The strongest 1555 cm^{-1} band must be assigned to ν_5 ($C_\alpha^I C_\alpha^I$ stretch coupled to the symmetric stretches of $C_\alpha C_m$ bonds), since this mode is calculated to be the highest skeletal mode in this region and have a quite high Raman intensity. The 1517 cm^{-1} band is assigned to ν_6 ($C_\alpha^{I,II} C_m$ asymmetric stretch coupled to the asymmetric half-ring stretch of Pyr-I). The Raman band at 1462 cm^{-1} is assigned to ν_8 ($C_\beta^I C_\beta^I$ stretch with strong coupling to $C_\alpha C_m$ symmetric stretch). We notice that the in-plane deformation of C_m-phenyls also contribute to this mode. The weak band at 1443 cm^{-1} is better assigned to ν_9 ($C_\beta^{II} C_\beta^{II}$ stretch in coupling with $C_\alpha C_m$ symmetric stretch).

Several phenyl modes are observed in the Raman spectra with notable intensities. The observed strong 1600 cm^{-1} band is assigned to the CC stretch of the phenyl groups (φ_4), which was calculated to appear at 1608 cm^{-1}. The middle-strong 1179 cm^{-1} Raman band corresponds to the 1179 cm^{-1} band in the theoretic spectrum and is assigned to the phenyl vibration involving mainly the phenyl CCH in-plane bending (φ_6). The weak band at 1579 cm^{-1} is thought to be a substituent mode involving the asymmetric CC stretch of

DOI:10.1063/1674-0068/26/04/398-408

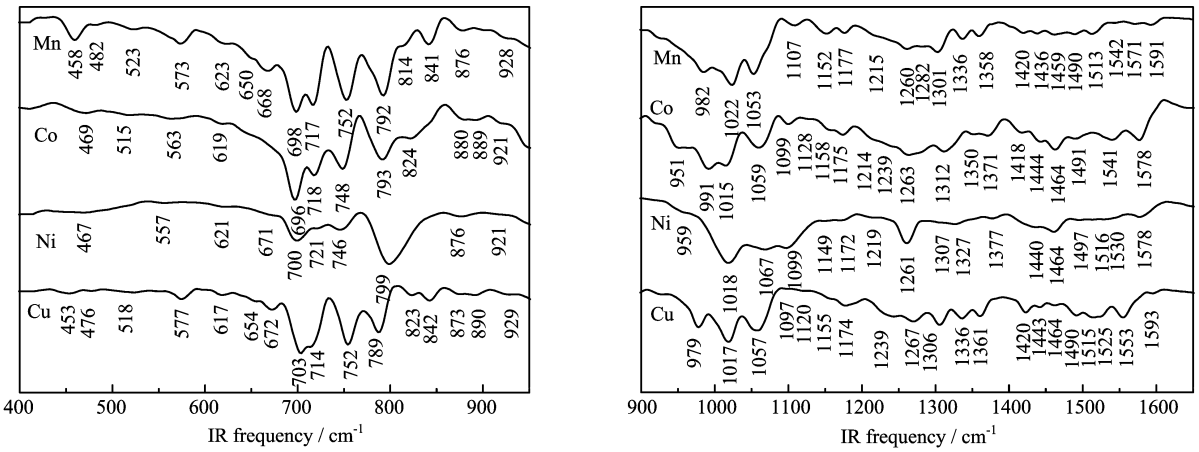

FIG. 4 Experimental IR absorption spectra (KBr discs) of CuTPC, NiTPC, CoTPC, and MnTPC.

phenyl groups (ψ_3), but corrole skeletal $C_\alpha C_m$ asymmetric stretch also contributes to this mode.

In the region of symmetric and asymmetric stretch of pyrrole rings (950−1440 cm^{-1}), the strongest band was observed at 1345 cm^{-1}. The corresponding band is calculated at the same position and is assigned to ν_{12}, the quarter-ring stretch of Pyr-I conjoint with $C_\alpha^{I,II}C_m$ symmetric stretch. The strong band at 1235 cm^{-1} is thought to correspond to the calculated strong band at 1224 cm^{-1}. This band (ν_{17}) is assigned to the $C'_mC'_1$ stretch that is strongly coupled to the in-plane CCH bending of the phenyl groups. The observed 1077 cm^{-1} band is assigned to the $C_\beta^{II}H$ in-plane symmetric bending calculated at 1072 cm^{-1}. The observed 1380, 1317, and 1017 cm^{-1} bands in this region are assigned to ν_{44} (the quarter-ring stretch of Pyr-I), ν_{47} (symmetric half-ring stretch of Pyr-II), and ν_{54} (breathing of Pyr-II). The calculated frequencies of these modes are 1371 (ν_{44}), 1316 (ν_{47}), and 1025 cm^{-1} (ν_{54}), respectively.

Additional weak or shoulder bands in this region were observed at 1426, 1281, 1120, 1047, 1003, and 992 cm^{-1}. The 1426 cm^{-1} band is assigned to ν_{43} (symmetric $C_\alpha^{I,II}C_m$ stretch that is weakly coupled to the $C_\beta^{II}C_\beta^{II}$ stretch). The 1281 cm^{-1} band in the experimental spectrum is assigned to ν_{15} (asymmetric $C_\beta^{I}H$ in-plane bending coupled to the quarter-ring stretch of Pyr-I). The ν_{43} and ν_{15} modes are calculated as 1428 and 1276 cm^{-1} with weak intensities. The weak bands at 1120 and 1047 cm^{-1} in the experimental spectrum are assigned to ν_{51} (the asymmetric $C_\beta^{I}H$ in-plane bending) and φ_7 (phenyl CH bending), respectively. Both ν_{51} and φ_7 have very low Raman intensities according to the calculation.

The Raman bands associating the pyrrole in-plane deformation, pyrrole rotational, pyrrole translational, pyrrole out-of-plane folding, pyrrole out-of-plane tilting and swiveling are expected to appear in the region lower than 950 cm^{-1}. Quite strong Raman bands were observed at 889, 845, and 831 cm^{-1}. The 889 cm^{-1} band can be assigned to γ_1 calculated at 881 cm^{-1}, which is a skeletal mode involving the asymmetric $C_\beta^{II}H$ out-of-plane wag. The 845 and 831 cm^{-1} bands are thought to come from the CH out-of-plane wag of phenyl groups (σ_2) and the in-plane deformation of the pyrroles (ν_{27}), respectively. The calculated frequencies of σ_2 and ν_{27} are 839 and 835 cm^{-1}, respectively, and both modes are of considerable Raman intensities. The weak bands observed at 921 and 903 cm^{-1} are thought to correspond to the calculated bands at 913 cm^{-1} (π'_2) and 889 cm^{-1} (ν_{57}), respectively. The former is due to the out-of-plane CH wag of C_m-phenyl groups, while the later is a corrole skeletal mode associating with the in-plane deformation of Pyr-I. The weak band at 787 cm^{-1} is assigned to γ_4 calculated at 762 cm^{-1} (symmetric out-of-plane folding of Pyr-I).

In the region lower than 800 cm^{-1}, Raman bands observed at 753, 655, 289, and 249 cm^{-1} are considered to be the out-of-plane skeletal vibrations, which were predicted at 755 cm^{-1} (γ_{19}), 647 cm^{-1} (γ_8), 300 cm^{-1} (γ_{11}), and 250 cm^{-1} (γ_{12}), respectively. The γ_{19} and γ_8 modes are assigned to the symmetric and asymmetric oop folding of Pyr-I, respectively. The γ_{11} mode is assigned to the swiveling of Pyr-II, while γ_{12} is due to the pyrrole tilting motions (*i.e.*, saddling of corrole macrocycle). The observed 314 cm^{-1} band is assigned to the in-plane skeletal mode ν_{33} (calculated at 313 cm^{-1}).

Raman bands at 701, 485, and 410 cm^{-1} in the experimental spectrum are assigned to phenyl out-of-plane CCC deformation vibrations π'_4, π'_5, and σ'_3. The calculated frequencies of these modes are 694 (π'_4), 486 (π'_5), and 406 cm^{-1} (σ'_3), respectively.

C. Comparison NiTPC with CoTPC, CuTPC and MnTPC

Figure 4 shows the infrared absorption spectra of MTPCs (M=Cu, Ni, Co, and Mn). It can be seen that the IR spectra of the four complexes are quite similar to each other. Some significant dif-

DOI:10.1063/1674-0068/26/04/398-408

TABLE VI Observed Raman frequencies (in cm^{-1}) of MTPCs and their assignments[a].

	NiTPC	CuTPC	CoTPC	MnTPC		NiTPC	CuTPC	CoTPC	MnTPC
φ_4	1600	1596	1600	1594	σ_1	962		953	
ψ_3	1579	1559	1582	1572	π_2'	921		921	918
ν_5	1555	1521	1564	1537	ν_{57}	903		901	898
ν_6	1517	1509	1534	1514	γ_1	889	888	885	882
ν_7	1504	1495	1507	1493	σ_2	845	844	845	842
ν_{40}	1493	1485			ν_{27}	831	822	831	829/815
ν_8	1462	1462	1473	1474	γ_4	787	783	785	794
ν_9	1443	1438		1435	γ_{19}	753	747	747	751
ν_{43}	1426	1425		1423	π_3'	723	722	723	716
ν_{10}	1411	1404	1419		π_4'	701	698	699	698
ν_{44}	1380	1363	1370	1362	γ_8	655	653	661	652
ν_{12}	1345	1340		1347	γ_{23}	637	631	642	643
ν_{47}	1317	1302	1328	1330	ψ_9'		618		625
ν_{14}	1298	1292		1302	γ_{24}	588	589	592	576
ν_{15}	1281	1263	1288	1263	γ_9	566	547	560	557
ν_{17}	1235	1235	1236	1235	ν_{28}	506	512	517	523
ν_{49}		1218		1219	π_5'	485	470	450	457
φ_6	1179	1186	1186	1176	ν_{63}	434		427	423
ψ_7'		1172		1151	σ_3'	410	412	406	406
ν_{51}	1120			1116	ν_{32}		402	391	382
ν_{52}	1077	1072	1072	1074	ν_{64}	334	358	334	345
φ_7	1047	1044	1042	1055	ν_{33}	314	324		
ν_{54}	1017	1019	1019	1021	γ_{11}	289	307		305
ν_{23}	1003	1000		1002	γ_{28}			266	267
φ_8'	992	979	992	986	γ_{12}	249	245	243	249
					φ_{10}''	214	210	199	215

[a] Raman spectra obtained from solid powder. Excitation wavelength is 488 nm.

ferences in the IR spectra of MTPCs are as follows. The CC stretch of C_m-phenyls (φ_4') were clearly observed in CuTPC (1593 cm^{-1}) and MnTPC (1591 cm^{-1}), but it was masked by nearby strong band (1578 cm^{-1}) in NiTPC and CoTPC. The IR bands at 1420/1418/1420, 979/991/982, and 823/824/814 cm^{-1} for CuTPC/CoTPC/MnTPC were assigned to ν_{43} (the symmetric $C_\alpha^{I,II}C_m$ stretch), ν_{24} (breathing of Pyr-I), and ν_{59} (pyrrole in-plane deformation), respectively. These bands were not observed or extreme weak in NiTPC. The strong band of NiTPC at 799 cm^{-1} is assigned to the ν_{60} mode. This mode was observed at 789/793/792 cm^{-1} in CuTPC/CoTPC/MnTPC, showing evident shift for different complexes. The middle strong band at 842/841 cm^{-1} in CuTPC/MnTPC were not observed in NiTPC and CoTPC. The band is assigned to γ_2, the out-of-plane $C_\beta^{II}H$ wag.

The 488 nm excited Raman spectra of MTPCs (M=Cu, Ni, Co, Mn) are displayed in Fig.5. As shown in Fig.5, the relative intensities of several Raman bands vary for different metal complexes, which is probably due to the different resonance enhancement pattern since the main electronic absorption of MTPCs, which varies from 415 nm to 440 nm, is not far from the laser line. In spite of this, Raman spectra of the four complexes show similar general trends and thus correlation of the corresponding bands of MTPCs can be made out as listed in Table VI. Some differences between the Raman spectra of the four complexes are noticed. For instance, the ν_{40} was observed in NiTPC and CuTPC but not in CoTPC and MnTPC while ν_{49} and ψ_7' were observed in CuTPC/MnTPC but not in NiTPC and CoTPC. The quality of the Raman spectrum of CoTPC is poorer as compared with others due to strong photolysis of the sample. Consequently, ν_9, ν_{43}, ν_{12}, ν_{14}, and ν_{23} of CoTPC were not observed due to the weak intensities.

The molecular structure changes generated by different metal substitutions can be reflected in the Raman spectra. For metalloporphyrins (MPors) and metallotetraazaporphyrins (MTAPs), empirical correlations have been found between the Raman frequencies and the core-size Ct-N (*i.e.*, the distance between the center of the porphyrin/tetraazaporphyrin ring and the pyr-

DOI:10.1063/1674-0068/26/04/398-408

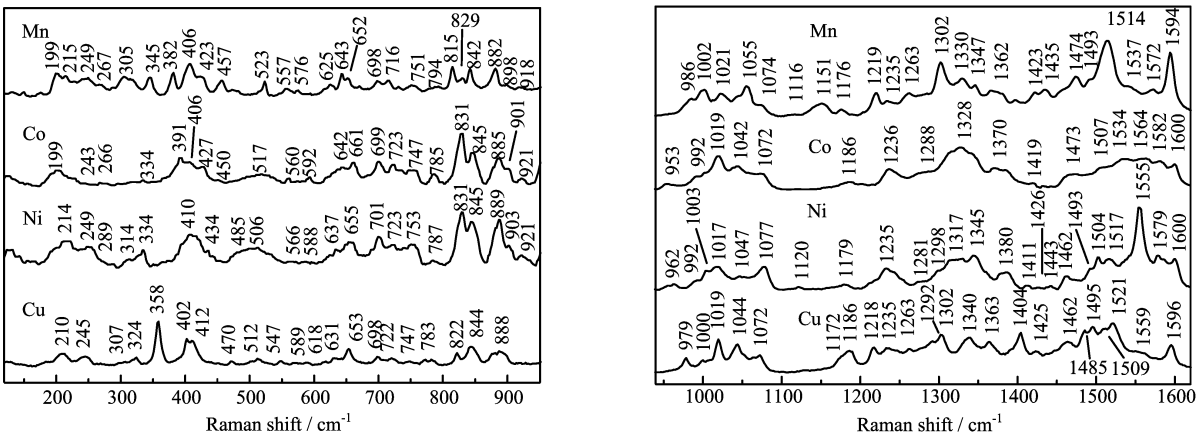

FIG. 5 Experimental Raman spectra (solid powder with 488 nm excitation) of CuTPC, NiTPC, CoTPC, and MnTPC.

role nitrogen atom) [25, 38, 39]. Especially, the Raman bands in the 1450−1600 cm^{-1} region, which are usually due to the stretching vibrations of the $C_\beta C_\beta$ and $C_\alpha C_m$ bonds, have been found sensitive to the core-size change.

We have studied the frequency/core-size relationship of MTPC by correlating the some observed Raman frequencies in the 1450−1600 cm^{-1} region with the DFT calculated M−N distances (averaged over four M−N bonds). Figure 6 displays the relationships between the core-sizes (M−N distances) and the frequencies of ν_5, ν_6, ν_7, and ψ_3 modes as well as the linear fitting of corresponding data. It is found that, in general, the Raman frequencies of these modes decrease with the increase of M−N distance. The slope of the fitted line reflects the relative sensitivity of a specific vibrational frequency to the core-size change. We found that with the decrease of core-size by 0.01 Å, the frequencies of ν_5, ν_6, ν_7, and ψ_3 increase by 6.76, 3.31, 2.23, and 3.48 cm^{-1}, respectively.

Among these four modes, ν_5 has the highest sensitivity and best linearity for its frequency/core-size relationship and thus can be used as a structure mark band for the corrole compounds. This mode is assigned to $C_\alpha^I C_\alpha^I$ stretch which is strongly coupled to the symmetric $C_\alpha^{I,II} C_m$ and $C_\alpha^{II} C'_m$ stretches. The ν_6 and ν_7 are assigned to the asymmetric $C_\alpha^{I,II} C_m$ stretch and symmetric $C_\alpha^{II} C'_m$ stretch, respectively. As a phenyl mode, the core-size dependent of ψ_3 is unusual. We find that while ψ_3 is nominally assigned to a phenyl mode, it contains a considerable component of asymmetric stretches of $C_\alpha^{I,II} C_m$ and $C_\alpha^{II} C'_m$. We consider that this vibrational coupling between substituents and corrole skeleton is partly responsible for the core-size dependent of ψ_3. In view that the $C_\alpha^I C_\alpha^I$ and $C_\alpha C_m$ stretches are sensitive to the core-size change, it can be deduced that the corrole macrocycle accommodates the metal ions with different sizes by adapting the $C_\alpha^I C_\alpha^I$ and $C_\alpha C_m$ bonds.

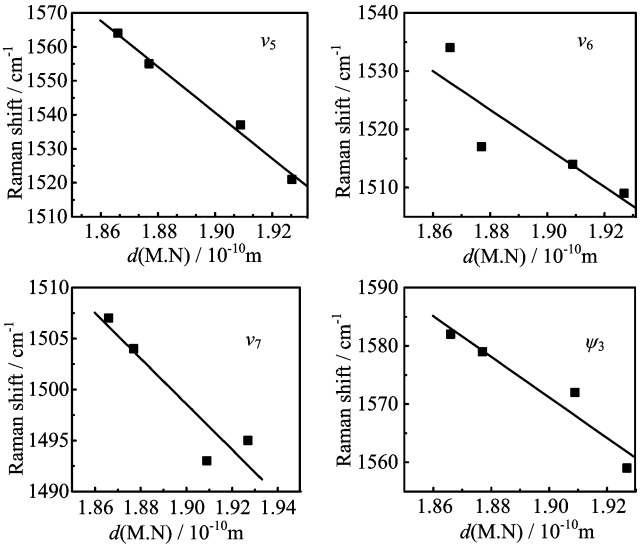

FIG. 6 Correlation between the Raman frequencies (for ν_5, ν_6, ν_7, and ψ_3 modes) and the calculated core-sizes of MTPC (M=Cu, Ni, Co, Mn). Frequencies from solid spectra excited at 488.0 nm.

IV. CONCLUSION

We have studied the IR absorption and 488 nm exited Raman scattering spectra of serious metal complexes of triphenylcorrole (MTPCs, M=Cu, Ni, Co, Mn). Density functional theory calculation using B3LYP functional were carried out to reveal the ground-state structures and vibrational states of MTPCs. Assignments of the observed IR and Raman bands of MTPCs to local coordinates were proposed based on the DFT calculations. Due to the symmetry lowing, the vibrational spectra of MTPCs are much more complex as compared with their porphyrin counterparts MTPP. The relationship between the Raman/IR frequencies and the structure of corrole ring was investigated. It was found that the vibrations involving the $C_\alpha^I C_\alpha^I$ stretch and $C_\alpha C_m$

DOI:10.1063/1674-0068/26/04/398-408

stretch are sensitive to the size of corrole core. The frequency of ν_5 increases linearly with the decrease of the corrole core-sizes and may be used as a mark to evaluate the structural change of the metallocorroles.

V. ACKNOWLEDGMENTS

This work was supported by the National Education Department of China (No.200803580022) and the Supercomputation Center of University of Science and Technology of China.

[1] S. Licoccia and R. Paolesse, Struct. Bonding **84**, 71 (1995).
[2] I. Aviv and Z. Gross, J. Chem. Commun. **20**, 1987 (2007).
[3] I. Aviv-Harel and Z. Gross, Chem. Eur. J. **15**, 8382 (2009).
[4] S. Will, J. Lex, E. Vogel, V. A. Adamian, E. Vancaemelbecke, and K. M. Kadish, Inorg. Chem. **35**, 5577 (1996).
[5] E. Vogel, S. Will, A. S. Tilling, L. Neumann, J. Lex, E. Bill, A. X. Trautwein, and K. Wieghardt, Angew. Chem. **106**, 731 (1994).
[6] Z. Gross, J. Biol. Inorg. Chem. **6**, 733 (2001).
[7] K. M. Kadish, J. Shen, L. Frémond, P. Chen, M. E. Ojaimi, M. Chkounda, C. P. Gros, J. M. Barke, K. Ohkubo, S. Fukuzumi, and R. Guilard, Inorg. Chem. **47**, 6726 (2008).
[8] Z. Gross and H. B. Gray, Adv. Synth. Catal. **346**, 165 (2004).
[9] A. Mahammed and Z. Gross, J. Am. Chem. Soc. **127**, 2883 (2005).
[10] S. Bose, A. Pariyar, A. N. Biswas, P. Das, and P. Bandyopadhyay, Catal. Commun. **12**, 446 (2011).
[11] A. N. Biswas, P. Das, A. Agarwala, D. Bandyopadhyay, and P. Bandyopadhyay, J. Mol. Catal. A **326**, 94 (2010).
[12] E. Vancaemelbecke, S. Will, M. Autret, V. A. Adamian, J. Lex, J. P. Gisselbrecke, M. Gross, E. Vogel, and K. M. Kadish, Inorg. Chem. **35**, 184 (1996).
[13] R. Misra, R. Kumar, V. PrabhuRaja, and T. K. Chandrashekar, J. Photochem. PhotoBiol. A **175**, 108 (2005).
[14] J. Shen, M. El Ojaimi, M. Chkounda, C. P. Gros, J. M. Barbe, J. Shao, R. Guilard, and K. M. Kadish, Inorg. Chem. **47**, 7717 (2008).
[15] E. Steene, T. Wondimagegn, and A. Ghosh, J. Am. Chem. Soc. **125**, 16300 (2003).
[16] (a) K. E. Thomas, I. H. Wasbotten, and A. Ghosh, Inorg. Chem. **47**, 10469 (2008).
(b) Addition and Correction: K. E. Thomas, I. H. Wasbotten, and A. Ghosh, Inorg. Chem. **48**, 1257 (2009).
[17] I. H. Wasbotten, T. Wondimagegn, and A. Ghosh, J. Am. Chem. Soc. **124**, 8104 (2002).
[18] E. Steene, T. Wondimagegn, and A. Ghosh, J. Inorg. Biochem. **88**, 113 (2002).
[19] Q. Z. Lu, Y. Lu, and J. J. Wang, Chin. J. Chem. Phys. **19**, 227 (2006).
[20] Y. T. Liao, H. Y. Rao, F. F. Kong, and M. B. Luo, Chin. J. Chem. Phys. **18**, 750 (2005).
[21] T. S. Rush III, P. M. Kozlowski, C. A. Piffat, R. Kumble, M. Z. Zgierski, and T. G. Spiro, J. Phys. Chem. B **104**, 5020 (2000).
[22] R. E. Oakes and S. E. J. Bell, J. Phys. Chem. A **107**, 10953 (2003).
[23] Y. H. Zhang, W. Zhao, J. Wang, and P. Jiang, Spectrochim. Acta **A75**, 499 (2010).
[24] Y. H. Zhang, W. Zhao, P. Jiang, L. J. Zhang, T. Zhang, and J. Wang, Spectrochim. Acta **A75**, 880 (2010).
[25] T. T. Lu, H. L. Gao, T. J. He, F. C. Liu, and D. M. Chen, Chin. J. Chem. Phys. **23**, 573 (2010).
[26] A. Alemayehu, J. Conradie, and A. Ghosh, Eur. J. Inorg. Chem. **12**, 1857 (2011).
[27] A. B. Alemayehu, L. K. Hansen, and A. Ghosh, Inorg. Chem. **49**, 7608 (2010).
[28] S. Ye, T. Tuttle, E. Bill, L. Simkhovich, Z. Gross, W. Thiel, and F. Neese, Chem. Eur. J. **14**, 10839 (2008).
[29] O. Zakharieva and C. Veeger, J. Molec. Struct. Theochem **723**, 171 (2005).
[30] H. L. Gao, G. H. Yao, F. Chen, W. L. Wang, and D. M. Chen, Chin. J. Chem. Phys. **25**, 281 (2012).
[31] B. Koszarna and D. T. Gryko, J. Org. Chem. **71**, 3707 (2006).
[32] K. M. Kadish, J. Shen, L. Frmond, P. Chen, M. E. Ojaimi, M. Chkounda, C. P. Gros, J. M. Barbe, K. Ohkubo, S. Fukuzumi, and R. Guilard, Inorg. Chem. **47**, 6726 (2008).
[33] (a) A. D. Becke, J. Chem. Phys. **98**, 5648 (1993).
(b) C. Lee, W. Yang, and R. G. Parr, Phys. Rev. B **37**, 785 (1988).
[34] (a) A. Schaefer, H. Horn, and R. Ahlrichs, J. Chem. Phys. **97**, 2571 (1992).
(b) A. Schaefer, C. Huber, and R. Ahlrichs, J. Chem. Phys. **100**, 5829 (1994).
[35] M. J. Frisch, G. W. Trucks, H. B. Schlegel, G. E. Scuseria, M. A. Robb, J. R. Cheeseman, G. Scalmani, V. Barone, B. Mennucci, G. A. Petersson, H. Nakatsuji, M. Caricato, X. Li, H. P. Hratchian, A. F. Izmaylov, J. Bloino, G. Zheng, J. L. Sonnenberg, M. Hada, M. Ehara, K. Toyota, R. Fukuda, J. Hasegawa, M. Ishida, T. Nakajima, Y. Honda, O. Kitao, H. Nakai, T. Vreven, J. A. Jr. Montgomery, J. E. Peralta, F. Ogliaro, M. Bearpark, J. J. Heyd, E. Brothers, K. N. Kudin, V. N. Staroverov, T. Keith, R. Kobayashi, J. Normand, K. Raghavachari, A. Rendell, J. C. Burant, S. S. Iyengar, J. Tomasi, M. Cossi, N. Rega, J. M. Millam, M. Klene, J. E. Knox, J. B. Cross, V. Bakken, C. Adamo, J. Jaramillo, R. Gomperts, R. E. Stratmann, O. Yazyev, A. J. Austin, R. Cammi, C. Pomelli, J. W. Ochterski, R. L. Martin, K. Morokuma, V. G. Zakrzewski, G. A. Voth, P. Salvador, J. J. Dannenberg, S. Dapprich, A. D. Daniels, O. Farkas, J. B. Foresman, J. V. Ortiz, J. Cioslowski, and D. J. Fox, *Gaussion 09*, Wallingford CT: Gaussian, Inc., (2010).
[36] X. Y. Li, R. S. Czernuszewicz, J. R. Kincaid, Y. O. Su, and T. G. Spiro, J. Phys. Chem. **94**, 31 (1990).
[37] X. Y. Li, R. S. Czernuszewicz, J. R. Kincaid, P. Stein, and T. G. Spiro, J. Phys. Chem. **94**, 47 (1990).
[38] W. A. Oertling, A. Salehi, Y. C. Chung, G. E. Leroi, C. K. Chang, and G. T. Babcock, J. Phys. Chem. **91**, 5887 (1987).
[39] N. Parthasarathi, C. Hansen, S. Yamaguchi, and T. G. Spiro, J. Am. Chem. Soc. **109**, 3865 (1987).

DOI:10.1063/1674-0068/26/04/398-408